International Journal of Control, Automation and Systems 14(6) (2016) 1535-1549
http://dx.doi.org/10.1007/s12555-014-0546-x
ISSN:1598-6446 eISSN:2005-4092
http://www.springer.com/12555

A Monocular Structured Light Vision Method for Pose Determination of Large Non-cooperative Satellites

Xue-Hai Gao, Bin Liang*, Le Pan, Zhi-Heng Li, and Ying-Chun Zhang

Abstract: A space robotic system is expected to perform on-orbit servicing missions to rescue malfunctioned satellites in geostationary orbit (GEO). In final berthing and capture, it is difficult for a space robot to determine the relative pose (attitude and position) of a non-cooperative malfunctioned satellite that is usually huge and without artificial recognition devices. In this paper, a space robot with a monocular structured light vision subsystem is introduced to solve the problem. Firstly, the monocular structured light vision subsystem composed of a single camera and a point light source is designed. Secondly, a partial rectangular shaped framework, which is very common on a non-cooperative malfunctioned satellite, is chosen as the recognition object for non-cooperative pose measurement. Using projection constraints on rectangle and circular points, a rectangle feature reconstruction algorithm is proposed. Thirdly, according to the reconstructed rectangle feature, a least square method of pose determination is presented. Lastly, using a semi-physical vision simulation system, several experiments of typical cases are simulated to verify the pose determination method of large non-cooperative target. The results show the validity and flexibility of the proposed method.

Keywords: Monocular vision, non-cooperative target, pose determination, space robot, structured light.

1. INTRODUCTION

In recent years, because the failures of high-value satellites happen frequently in GEO, more and more attentions have been paid to the on-orbit servicing (OOS) of GEO. Many countries and organizations have been researching and developing the OOS technologies, including repairing, upgrading, refueling and re-orbiting spacecraft on-orbit. These technologies could potentially extend the life of satellites, enhance the capability of space systems, reduce the space operation costs, and clean up the increasing space debris [1].

Space robotic systems are expected to play an increasingly important role in OOS [2]. Several space robotic systems of GEO have been conceptually designed by some organizations. The Germany space agency (DLR) has proposed the Experimental Servicing Satellite (ESS) to repair failed satellites in GEO [3]. The TV-SAT-1 which failed to unfold one of solar panels was chosen as the target satellite for a prototype scenario. The European Space Agency (ESA) has designed the Geostationary Service Vehicle (GSV) which was intended to provide on-orbit inspection and intervention with GEO satellites [4]. Three types of intervention were identified: inspection of a satellite with severe malfunction, mechanical assistance to a satellite in trouble and re-orbiting an uncontrolled satellite into a graveyard orbit. The Orbital Recovery Corporation has presented the novel concept of ConeXpress Orbital Life Extension Vehicle (CX-OLEV) to significantly prolong the operating life-time of communication satellites in GEO [5]. The CX-OLEV will supply the propulsion, navigation and guidance to keep a communication satellite in its proper orbit and rescue the spacecraft that has been placed in a wrong orbit. Another important on-orbit servicing concept is the Spacecraft for Universal Modification of Orbits (SUMO) [6]. The purpose of the program is to demonstrate the integration of machine vision, robotics, mechanisms and autonomous control algorithms to accomplish autonomous rendezvous and also the grapple of a variety of interfaces traceable to future OOS operations. The Micro-satellite Technology Experiment (MiTEx) of Defense Advanced Research Projects Agency (DARPA) has been used to inspect the DSP-23, a failed missile detection satellite of GEO, to find out why it stopped operating.

To service a malfunctioned satellite in GEO, the space

Manuscript received December 12, 2014; revised July 21, 2015; accepted December 15, 2015. Recommended by Associate Editor Gon-Woo Kim under the direction of Editor Duk-Sun Shim. This work was supported by the National Nature Science Foundation of China (No. 61305112, 61473297).

Xue-Hai Gao, Bin Liang, and Zhi-Heng Li are with the Center of Intelligent Control and Telescience, Graduate School at Shenzhen, Tsinghua University, the Xili University Town, Shenzhen 518055, China (e-mails: xuehaigao@163.com, bliang@tsinghua.edu.cn, zhhli@tsinghua.edu.cn). Le Pan and Ying-Chun Zhang are with the Shenzhen Aerospace Dongfanghong HIT Satellite Ltd. Satellite Building, 2002 Keyuan Street, Nanshan District, Shenzhen 518057, China (e-mails: verapanle@163.com, zhang@hit.edu.cn).
* Corresponding author.

robotic systems should have the ability of autonomous rendezvous. Especially, in final berthing and capture, the pose determination of a non-cooperative malfunctioned target is a key technology for a space robot. Vision based system is commonly used to measure the relative attitude and position [7–9]. The Proximity Sensor (PXS) system of the Engineering Test Satellite-VII (ETS-VII of Japan) and the Advanced Video Guidance Sensor (AVGS) system of the Orbital Express (OE of USA) are vision based systems for pose measurement. The two vision based systems depend on the corner-cubes mounted on the target satellites to work, i.e., the operated target satellites are cooperative. However, the existing satellites of GEO were not specially designed to be serviced. These satellites are non-cooperative targets, i.e., neither artificial features for pose measurement nor advanced mechanisms for capture were mounted on these satellites. Therefore, without cooperative information, it is a challenge for a space robot to determine the pose of a target satellite in final berthing and capture. Lichter and Dubowsky proposed a new architecture for the estimation of dynamic state, geometric shape and model parameters of objects in orbit [10]. The method required a team of cooperative 3D vision sensors to work at different positions. The method seemed to be a costly and burdened operation for space missions. Jasiobedski *et al*. presented a new concept of vision system for proximity operations of satellite [11]. The system processed images from stereo cameras to perform pose determination and tracking. Terui *et al*. developed an algorithm for estimating the motion of failed satellites by using stereo visions [12]. However, the size of target satellites are usually huge, these stereo cameras can not photograph the whole targets and fail to estimate their relative pose. Du *et al*. proposed a collaborative cameras system to measure the pose of a large non-cooperative satellite by using a rectangle feature [13]. Xu *et al*. also designed a binocular stereo vision system to determine the pose of a target satellite by using a circle feature [14]. But the two systems may exist reliability risks. If one of the two cameras is in trouble, the pose measurement will fail. Therefore, a reasonable and reliable vision system should be developed for the pose measurement of large non-cooperative satellites.

In this paper, a space robot with a monocular structured light vision subsystem is introduced to determine the pose of large non-cooperative satellites. Before designing the vision system, it is necessary to seriously study the target satellites to determine the recognition objects. Based on the survey of existing satellites, nature rectangular features that are common in the configuration of target satellites are used for pose measurement. Then, a monocular structured light vision system composed of a single vision camera and a point light source is designed in detail. A pose measurement algorithm is proposed based on a partial rectangle feature of target satellites. Using projection constraints on rectangle and circular points, a virtual whole rectangle can be reconstructed by the image of the partial rectangle and the point light. Using least square method, the attitude and position of target satellite is derived from the virtual whole rectangle. And a semi-physical vision simulation system is established to verify the proposed method.

2. A TYPICAL OOS SPACE ROBOTIC SYSTEM FOR LARGE NON-COOPERATIVE SATELLITES

2.1. The serviced non-cooperative satellites

From the report of ESA [15], only 32% GEO spacecrafts are controlled operational satellites. Especially, the communication satellites which are high-value and important are often out of order. Three communication satellites with failure are shown in Fig. 1. Failed to deploy its solar arrays and communication antennas, the SINOSAT-2 lost its function totally and its status is free-floating. Because of solar arrays problems, the NIGCOMSAT-1 also lost its function totally and its status is also free-floating. As a result of the under-performance during its launch, the INSAT-4CR had to expend manoeuvring and station keeping propellant to raise its orbit by more than had originally been planned. And the operational lifetime of the satellite was reportedly decreased by up to five years. The three communication satellites with failures are non-cooperative target satellites to be serviced. Because

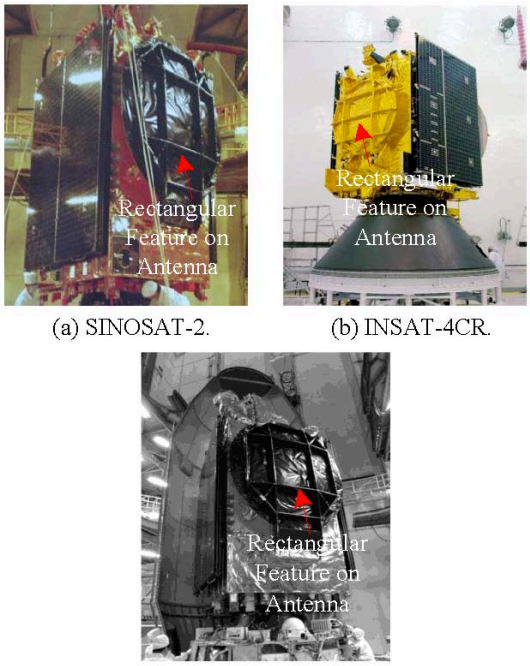

(a) SINOSAT-2. (b) INSAT-4CR.

(c) NIGCOMSAT-1.

Fig. 1. The communication satellites with failures in GEO.

these satellites are non-cooperative, only natural features can be chosen as measurement objects for pose measurement. According to the investigation of these communication satellites, it is found that there always exist frameworks on the backboard of antennas that can increase the strength of structure. These frameworks can be taken as the feature for pose measurement. Fig. 1 shows the test status of the three communication satellites in testing hall. As seen from these pictures, rectangular features are very common in the framework. Consequently, it is of great significance to perform the pose determination by recognizing the rectangular structure. In order to further study on pose measurement of non-cooperative target satellite in detail, the SINOSAT-2 is taken as the specific example. The failure cases of the communication satellite are shown in Fig. 2(A). It includes three failures during its on-orbit deploying: (A1) Failed to deploy the -Y solar arrays. (A2) Failed to deploy the +X antenna. (A3) Failed to deploy the -X antenna. And the rectangular structure on the unfolded antenna is chosen as the recognition feature.

2.2. The OOS space robotic system

Many advanced space robotic technologies have been demonstrated in Low Earth Orbit (LEO). And a few unmanned OOS missions of satellite maintenance have been performed. With the development of space robotic technology, the space robotic system is expected to play an increasingly important role in repairing malfunctioned satellites of GEO.

The functions of a space robotic system include rendezvous, berthing, capture and repair. The berthing and capture of the SINOSAT-2 by a space robotic system is shown in Fig. 2. The conceptual space robotic system is presented in Fig. 2(B). It is mainly composed of the following parts:

(B1) Two 7-DOF (degree of freedom) manipulators with 7 serial revolution joints. Because of the huge size of the target satellite, the two manipulators can expand operation area. The operation manipulator is with two hand-eye cameras and a replaceable end-effector. It is used to repair the target satellite, for example, to deploy the unfolded mechanisms, transfer and install ORUs (Orbital replaceable unit), and so on. The capture manipulator is with berthing and latching mechanism. It is used to capture the target satellite and form rigid combination body, for example, the apogee engine nozzle. Compared with its 6-DOF counterpart, the 7-DOF redundant manipulator is very flexible for singularities handling, obstacle avoiding, tumbling satellites capturing, etc.

(B2) Relative navigation and measurement subsystem. The subsystem includes a set of laser range finder, narrow field of view camera, structured light vision devices and illumination devices. The subsystem, mounted on the +X panel of the space robotic system, is used to supply the relative position and velocity during the far rendezvous, the

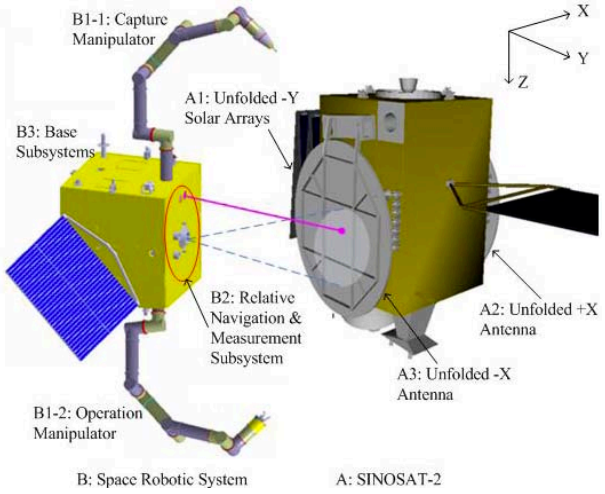

Fig. 2. The berthing and capture of SINOSAT-2 by a space robotic system.

relative pose during the close approaching and berthing at the berthing point, where the capture manipulator can reach the apogee engine nozzle of target. The subsystem is one of the key techniques for autonomous rendezvous and berthing.

(B3) Base subsystems. Guidance, Navigation and Control (GNC) subsystem is one of the most important base subsystems. It is controlled to rendezvous with target in the desired attitude and position. The control loops for attitude and trajectory control include the sensors for position and attitude measurement, the GNC functions, the thrusters and wheel actuators for attitude and position control. The base subsystems also have the planner and controller of the two 7-DOF manipulators. The main function of the planner is to plan the motions of manipulator according to different tasks, for example, the berthing task and repair task. The planner outputs the desired joint angles and rates. Then, each joint controller interposes more path nodes between the current values and the desired values, and drives each joint to track the desired motion. In addition to those mentioned above, the base subsystems also have the necessary parts as other spacecrafts, such as the structure, power, TT&C, and so on.

This section introduces the serviced target satellite and the space robotic system. In final berthing and capture, the pose determination of the non-cooperative target satellite is one of the key technologies. The method will be proposed in the following sections.

3. THE DESIGN OF MONOCULAR STRUCTURED LIGHT VISION SENSOR

3.1. The design of measurement sensor system

The monocular structured light vision sensor is part of the relative navigation and measurement subsystem. It is used to determine the relative pose between the space

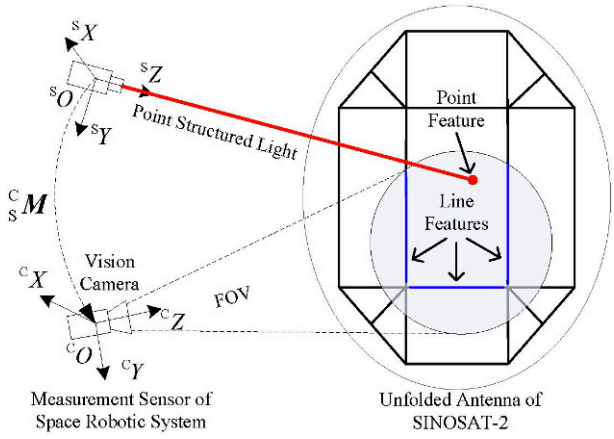

Fig. 3. The configuration of the monocular structured light vision sensor.

robotic system and the non-cooperative target satellite in final berthing and capture. In section 2.1, the rectangular feature of unfolded antenna is taken as the feature for pose measurement. Because of the huge size of the non-cooperative target satellite, a monocular camera limited by field of view (FOV) can not obtain the whole rectangular feature to compute the relative pose. Therefore, a point light source is introduced to the camera to compose the monocular structured light vision sensor system to solve the problem. The configuration of the monocular structured light vision sensor is shown in Fig. 3. The point light can form a point on the rectangular feature. And the point is always in the FOV of the camera. Then, the camera can obtain a point and three line features of the rectangular featrue to determine relative pose. Vision cameras that are low mass, low energy requirement and low cost are commonly used in current space robotic systems. A feasible camera should be designed to recognize the rectangular feature. Usually, the size of communication satellites are very huge. The area of antenna on the SINOSAT-2 is about 3000 mm $\times$ 2200 mm. The length and width of middle rectangular structure are about 1200 mm and 77 0mm. If a monocular camera is applied in the range of final approach, it will have a sufficient wide FOV to photograph the whole rectangle at berthing position (1 meter away from the rectangle). By geometric calculation, the theoretical FOV of the camera is about 62°. It is assumed that the maximum error of attitude control is about $\pm 5°$, and a margin of the FOV for redundancy is considered as 7°. Then, the practical FOV of the camera will be at least 80°. As well known, the FOV of 80° will bring a significant lens distortion. In this situation, it is difficult to exactly extract the recognition feature.

For the problem, the FOV of the camera is designed by the width of middle rectangle. Though the whole rectangle can not be extracted, the added point structured light can be combined to measure the relative pose. By the width of middle rectangle, the FOV of the camera is about 42°. Added the control error and the margin for redundancy, the practical FOV of the camera is about 55°. From 1.6m to 1m, the image of middle rectangle will be partial by the camera. A CCD array is selected as the optical sensor. The parameters of designed monocular camera are shown in Table 1. In the measurement sensor system, ${}^{\mathrm{C}}O-{}^{\mathrm{C}}X{}^{\mathrm{C}}Y{}^{\mathrm{C}}Z$ is the camera coordinate system. Its origin ${}^{\mathrm{C}}O$ is at the center of camera aperture. Axis ${}^{\mathrm{C}}Z$ is pointing to the line-of-sight (LOS) of camera and referred as the optical axis. Axes ${}^{\mathrm{C}}X$ and ${}^{\mathrm{C}}Y$ are parallel to the image plane that is located at the focus distance. Its coordinate is ${}^{\mathrm{C}}\boldsymbol{P} = [{}^{\mathrm{C}}X, {}^{\mathrm{C}}Y, {}^{\mathrm{C}}Z, 1]^{\mathrm{T}}$. ${}^{\mathrm{S}}O-{}^{\mathrm{S}}X{}^{\mathrm{S}}Y{}^{\mathrm{S}}Z$ is the point light coordinate system. The origin ${}^{\mathrm{S}}O$ is the origin of the point light. Axis ${}^{\mathrm{S}}Z$ is pointing to the emitting direction of the point light. Its coordinate is ${}^{\mathrm{S}}\boldsymbol{P} = [0, 0, {}^{\mathrm{S}}Z, 1]^{\mathrm{T}}$. The matrix ${}^{\mathrm{C}}_{\mathrm{S}}\boldsymbol{M}$ is the mounted matrix between the camera and the point light. It can be calibrated by the methods in [16, 17]. In camera coordinate system, the line of the point light can be described as:

$$ {}^{\mathrm{C}}\boldsymbol{P} = {}^{\mathrm{C}}_{\mathrm{S}}\boldsymbol{M}\,{}^{\mathrm{S}}\boldsymbol{P}. \tag{1} $$

In (1),

$$ {}^{\mathrm{C}}_{\mathrm{S}}\boldsymbol{M} = \begin{bmatrix} {}^{\mathrm{C}}_{\mathrm{S}}\boldsymbol{R} & {}^{\mathrm{C}}_{\mathrm{S}}\boldsymbol{T} \\ \boldsymbol{0} & 1 \end{bmatrix}. $$

${}^{\mathrm{C}}_{\mathrm{S}}\boldsymbol{R}$ is a 3x3 orthonormal unit rotation matrix. ${}^{\mathrm{C}}_{\mathrm{S}}\boldsymbol{T}$ is a 3x1 translation vector. These parameters can be calibrated exactly. It is assumed that the theoretical value are:

$$ {}^{\mathrm{C}}_{\mathrm{S}}\boldsymbol{R} = \begin{bmatrix} 1 & 0 & 0 \\ 0 & 1 & 0 \\ 0 & 0 & 1 \end{bmatrix}, \quad {}^{\mathrm{C}}_{\mathrm{S}}\boldsymbol{T} = [0,\ -500\ \mathrm{mm},\ 0]^{\mathrm{T}}. $$

Then, the monocular structured light vision measurement sensor system is developed.

Table 1. The parameters of designed camera.

	Parameter	Specification
(1)	FOV	55°
(2)	Focal length	13.5mm
(3)	Sensor type	CCD
(4)	Sensor size	1/2”
(5)	Pixel number	1024x1024

3.2. The application of measurement sensor system

The main procedure of the pose determination of the non-cooperative target satellite is shown in Fig. 4. It is composed of three steps: (a) Image acquisition including partial rectangle and point light. (b) Image processing including point detection and partial rectangle detection. (c) Pose determination including virtual rectangle reconstruction method and pose calculation algorithm.

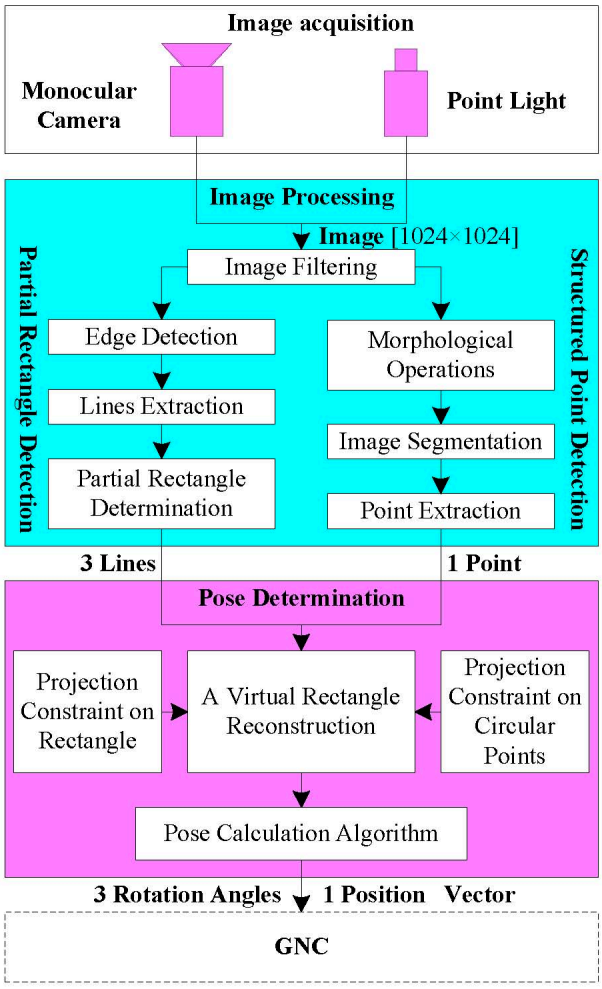

Fig. 4. The flowchart of pose determination for a non-cooperative target.

The results of image processing are the inputs of pose determination method. In order to theoretically verify the proposed method, the technology of computer image and graph is applied to generate an emulated image of the camera. The emulated image will be obtained by a industrial CCD camera of the semi-physical vision simulation system that will be introduced in Section 5. The models of space robot, target satellite and orbital environment are created by OpenGL (Open Graphics Library) which is a software interface to graphics hardware. A virtual camera is created by OpenGL to simulate gray images which are photographed by real cameras mounted on the space robot. The virtual camera has the same parameters as the designed real camera in Table 1. Noise will be introduced into the images via any electrical systems used for generation and transmission. Removing noise is the first step of image processing. According to the investigation of physical vision system, there exist the following four noises at least: (a) Thermal noise, arising from the thermal energy within the silicon lattice comprising the CCD. As the integration time increases, the number of thermal electrons increases. (b) On-chip electronic noise, originating in the process of reading the signal from sensor. (c) Amplifier noise, which is additive, is Gaussian and independent of signal. In modern well-designed electronics, the amplifier noise is generally negligible. (d) Quantization noise, which is inherent in the amplitude quantization process, occurs in the analogue-to-digital converter. It can be ignored by using a high-bit analogue-to-digital converter. Then, the total noise can be considered as an independent additive white Gaussian noise. An emulated gray image of partial antenna and point light added white Gaussian noise is shown in Fig. 5(a). The mean of white Gaussian noise is 20. The variance of white Gaussian noise is 100.

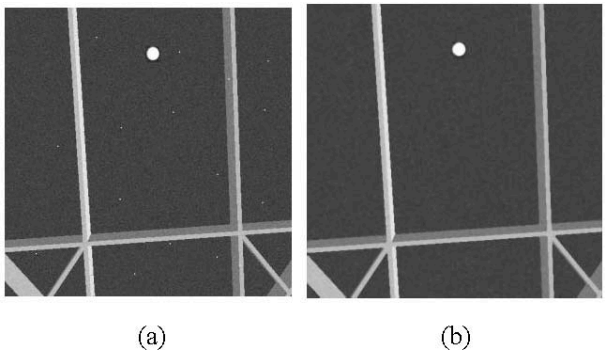

Fig. 5. (a) An emulated gray image of partial antenna with noise; (b) The image after Median Filtering.

Median Filtering is a simple and effective noise removal filtering process. Its performance is particularly good for removing shot noise which consists of strong spike-like isolated values. Median Filtering can smooth the data, while keeping the small and sharp details. It is quite appropriate for our image filtering process.

The template size of Median Filtering is selected as 5x5. After image filtering, the image processing includes structured point detection and partial rectangle detection, as shown in Fig. 5(b).

3.2.1 The structured point detection

A. Morphological Operations

By Otsu's Method, a global threshold that can be used to convert the gray image to a binary image is automatically computed. Below the threshold, the value of binary image is 0. Above the threshold, the value of binary image is 1. After that, the gray image will be transformed to a binary image to calculate the centers of different regions. Influenced by noise, some small noise pixels may exist in the background of the binary image. And the brims of the regions are generally not smooth and some small holes may be in the regions. In order to solve these questions, morphological operations are usually applied. The basic morphological operations are dilation and erosion. Opening operation (erosion-dilation) is used to elim-

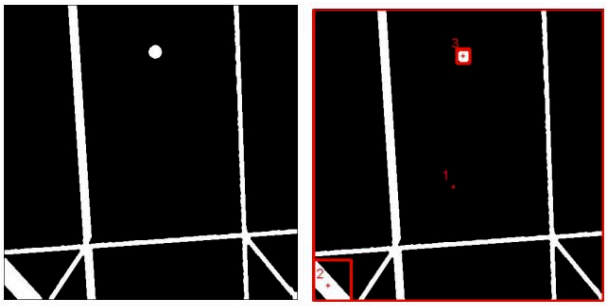

(a) (b)

Fig. 6. (a) The image after morphological operation; (b) The image after Segmentation operation.

inate noise pixels and smooth brims. Closing operation (dilation-erosion) is adopted to fill holes. The binary image is shown in Fig. 6(a).

B. Image Segmentation Operation

Region Segmentation is the way to get the highly similar pixels together and mark them in image processing. It is used to distinguish the different regions in an image. The structured point formed by the point light is a bright region in the binary image. This situation is very fit for the region segmentation. The seeded region growing segmentation which is more reliable is adopted. An initial seeded pixel is selected as the growing origination. Neighboring pixels whose gray levels are similar to the seeded pixel will be gathered into a same region. And the neighboring pixels become new seeded pixels to repeat the same process until no satisfied pixels. Then, the different regions based on the initial seeded pixel are grown out. After Segmentation, the binary image of Fig. 6(a) has three regions, as shown in Fig. 6(b). It will be used for computing the center pixel coordinate of the structured point.

C. Point Extraction

Through Segmentation operation, the binary image has different regions: the structured point and the other framework of antenna. Observing the binary image, the region of structured point is a convex set. The main property of convex set is that the connection between any two points of the set is always in the set. And the region of structured point is always at the upper middle of the binary image because of the installation location between the monocular camera and the point light. Therefore, the region of the structured point can be uniquely determined by the two characters. By marking, the coordinate of every pixel in the region of the structured point can be obtained. Then, the center of structured point $\boldsymbol{p}_5 = [u_5, v_5, 1]^{\mathrm{T}}$ can be computed by:

$$u_5 = \sum_{i=0}^{N} u_i/N, \quad v_5 = \sum_{i=0}^{N} v_i/N. \tag{2}$$

In (2), N is the number of pixels in the region of structured point and (u_i, v_i) are the corresponding pixel coordinate.

3.2.2 The partial rectangle detection

A. Canny Edge Detection

The Canny edge detection algorithm is known as the optimal edge detector. In this paper, it is used to detect edges of the filtered gray image. Firstly, the Canny edge detector smoothes the image to eliminate noise. Secondly, it finds the image gradient to highlight regions with highly spatial derivatives. Thirdly, it tracks these regions to perform non-maximum suppression which can reduce the gradient array. Then, the hysteresis is used to detect edges from the remaining pixels which have not been suppressed. It uses two low and high thresholds to find edges. If the magnitude of pixel is below the low threshold, it will be set to zero. If the magnitude of pixel is above the high threshold, it will be made an edge. And if the magnitude is between the two thresholds, it will be set to zero unless there exists a path from this pixel to another pixel with a gradient above the high threshold. The low threshold is set to 30. The high threshold is set to 130. The detected edges are shown in Fig. 7(a).

B. Hough Lines Extraction

After Edge Detection, the binary image which contains edge information is obtained. In order to recognize the sides of rectangle, Hough Transform is applied to extract the lines in the binary image. The Hough Transform maps points in Cartesian image space to curves in Hough polar coordinate space $\rho - \theta$ (distance-angle) [18], i.e.,

$$u\cos\theta + v\sin\theta = \rho. \tag{3}$$

In Hough polar coordinate space, the points which are collinear in Cartesian image space become readily apparent. The main advantage of Hough Transform technique is that it is tolerant of gaps in feature boundary descriptions and relatively unaffected by image noise. According to the Hough Transform, each point is transformed to a sinusoidal curve in the Hough polar coordinate space. If a group of points belong to a straight line, their corresponding sinusoidal curves will be intersected at a same point. Through the Hough Transform, all line segments can be extracted in the binary image. The parameters of Hough Transform are shown in Table 2.

C. Partial Rectangle Determination

Many lines may be extracted in the last procedure because of the complicated scene. Only three edges will be detected from the framework of the antenna. The middle lines will be selected as the sides of partial rectangle. To pick the three lines out, the extracted structured point is used as a reference point. Draw perpendicular line to all extracted line segments through the reference point, as shown in Fig. 7(b). The three lines will be determined by the reference point. And their Hough polar parameters

Table 2. The parameters of Hough transform.

	Parameter	Specification
(1)	Step length of ρ	1
(2)	Step length of θ	0.01745rad
(3)	Maximum gap of segment merging	50
(4)	Minimum length of segment	10
(5)	Minimum length of output	40

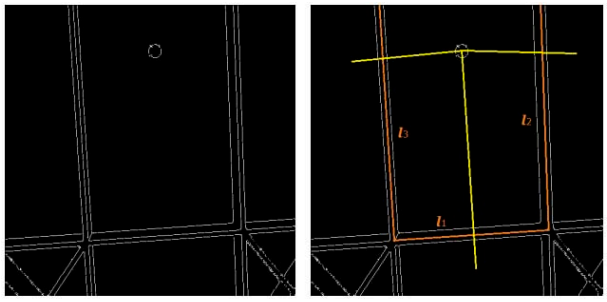

(a) (b)

Fig. 7. (a) The image after Canny edge detection; (b) The image after rectangle determination.

are: $\boldsymbol{l}_i(\rho_i,\theta_i), i=1,2,3$. Until now, the information of the structured point and the partial rectangle are obtained.

4. THE POSE DETERMINATION METHOD FOR LARGE NON-COOPERATIVE SATELLITES

Based on the information of the structured point and the partial rectangle, pose measurement algorithm will be proposed. The pose determination method has two steps: (a) The virtual rectangle reconstruction. (b) The pose calculation using the virtual rectangle. Firstly, the model and question of pose measurement based on the monocular structured light vision sensor will be introduced.

4.1. The model and question of pose measurement

The model of pose measurement is shown in Fig. 8. There are four coordinate systems in the model. The camera coordinate system ${}^{\mathrm{C}}O-{}^{\mathrm{C}}X{}^{\mathrm{C}}Y{}^{\mathrm{C}}Z$ and the point light coordinate system ${}^{\mathrm{S}}O-{}^{\mathrm{S}}X{}^{\mathrm{S}}Y{}^{\mathrm{S}}Z$ have been introduced in Section 3.1. ${}^{\mathrm{P}}O-uv$ is image coordinate system. Its coordinate is $\boldsymbol{p}=[u,v,1]^{\mathrm{T}}$. Its origin ${}^{\mathrm{P}}O$ is at the top left vertex of image plane. The axes u and v are along the top and left sides of image plane. (u_0,v_0) is the center of image plane. ${}^{\mathrm{T}}O-{}^{\mathrm{T}}X{}^{\mathrm{T}}Y{}^{\mathrm{T}}Z$ is target coordinate system. Its coordinate is ${}^{\mathrm{T}}\boldsymbol{P}=[{}^{\mathrm{T}}X,{}^{\mathrm{T}}Y,{}^{\mathrm{T}}Z,1]^{\mathrm{T}}$. The origin ${}^{\mathrm{T}}O$ is at the bottom left vertex of the partial rectangle. The axis ${}^{\mathrm{T}}Z$ is vertical to the plane of rectangle. The axes ${}^{\mathrm{T}}X$ and ${}^{\mathrm{T}}Y$ are along the bottom and left sides of the plane of rectangle. A camera can be described by Pin-hole model which is

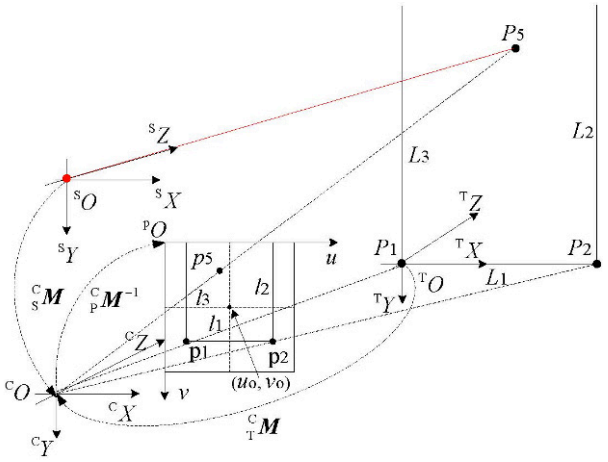

Fig. 8. The model of pose measurement based on the monocular structured light vision sensor.

a linear model. Then, the transformation between image coordinate and camera coordinate can be given by:

$$\lambda\boldsymbol{p}=[{}^{\mathrm{P}}_{\mathrm{C}}\boldsymbol{M}\quad\boldsymbol{0}]{}^{\mathrm{C}}\boldsymbol{P}. \tag{4}$$

In (4),

$$\lambda={}^{\mathrm{C}}Z,\quad {}^{\mathrm{P}}_{\mathrm{C}}\boldsymbol{M}=\begin{bmatrix} f/d_u & 0 & u_0\\ 0 & f/d_v & v_0\\ 0 & 0 & 1\end{bmatrix}.$$

${}^{\mathrm{P}}_{\mathrm{C}}\boldsymbol{M}$ determined by the parameters in Table 1 is the intrinsic parameters of camera. It can be exactly obtained by camera calibration [19–21]. f is the focus length of camera. d_u and d_v are the physical pixel pitch in direction of axes u and v.

Similar to (1), the relationship between target coordinate system and camera coordinate system can be described by:

$${}^{\mathrm{C}}\boldsymbol{P}={}^{\mathrm{C}}_{\mathrm{T}}\boldsymbol{M}{}^{\mathrm{T}}\boldsymbol{P}. \tag{5}$$

In (5),

$${}^{\mathrm{C}}_{\mathrm{T}}\boldsymbol{M}=\begin{bmatrix} {}^{\mathrm{C}}_{\mathrm{T}}\boldsymbol{R} & {}^{\mathrm{C}}_{\mathrm{T}}\boldsymbol{T}\\ \boldsymbol{0} & 1\end{bmatrix}.$$

${}^{\mathrm{C}}_{\mathrm{T}}\boldsymbol{R}=[{}^{\mathrm{C}}_{\mathrm{T}}\boldsymbol{r}_1,{}^{\mathrm{C}}_{\mathrm{T}}\boldsymbol{r}_2,{}^{\mathrm{C}}_{\mathrm{T}}\boldsymbol{r}_3]$ is a 3x3 orthonormal unit rotation matrix. ${}^{\mathrm{C}}_{\mathrm{T}}\boldsymbol{T}=[{}^{\mathrm{C}}_{\mathrm{T}}t_1,{}^{\mathrm{C}}_{\mathrm{T}}t_2,{}^{\mathrm{C}}_{\mathrm{T}}t_3]^{\mathrm{T}}$ is a 3x1 translation vector. Substituting (5) into (4), the relationship between target coordinate system and image coordinate system is:

$$\lambda\boldsymbol{p}=[{}^{\mathrm{P}}_{\mathrm{C}}\boldsymbol{M}\quad\boldsymbol{0}]{}^{\mathrm{C}}_{\mathrm{T}}\boldsymbol{M}{}^{\mathrm{T}}\boldsymbol{P}. \tag{6}$$

From (6), the question of pose measurement is to determine relative position and rotation angles between target coordinate system and camera coordinate system by using the image of partial rectangle feature and structured light. i.e., the question is to compute the transformation matrix

${}^{\mathrm{C}}_{\mathrm{T}}\boldsymbol{M}$. The relative position is ${}^{\mathrm{C}}_{\mathrm{T}}\boldsymbol{T}$. Defined that the Euler rotation sequence of coordinate system is $Z\rightarrow X\rightarrow Y$, and the corresponding rotation angle is $\gamma\rightarrow\alpha\rightarrow\beta$. Then, the Euler direction cosine transform matrix ${}^{\mathrm{C}}_{\mathrm{T}}\boldsymbol{R}$ will be:

$$ {}^{\mathrm{C}}_{\mathrm{T}}\boldsymbol{R}=\begin{bmatrix} C_\beta C_\gamma+S_\alpha S_\beta S_\gamma & -C_\beta S_\gamma+S_\alpha S_\beta C_\gamma & C_\alpha S_\beta \\ C_\alpha S_\gamma & C_\alpha C_\gamma & -S_\alpha \\ -S_\beta C_\gamma+S_\alpha C_\beta S_\gamma & S_\beta S_\gamma+S_\alpha C_\beta C_\gamma & C_\alpha C_\beta \end{bmatrix}. \tag{7} $$

In (7), S stands for sine. C stands for cosine.

4.2. The virtual rectangle reconstruction

Because the target satellite is non-cooperative and the size of partial rectangle feature is unknown, it is difficult to calculate the relative pose by the partial rectangle. Therefore, it is necessary to reconstruct a whole virtual rectangle. For this purpose, projection constraints on rectangle and circular points will be concluded.

4.2.1 The reconstruction of virtual rectangle in image coordinate system

If a point is on a plane, i.e., ${}^{\mathrm{T}}Z=0$, its target coordinate can be rewritten to ${}^{\mathrm{t}}\boldsymbol{P}=[{}^{\mathrm{T}}X,{}^{\mathrm{T}}Y,1]^{\mathrm{T}}$. equation (6) will be:

$$ \lambda\boldsymbol{p}={}^{\mathrm{p}}_{\mathrm{C}}\boldsymbol{M}[{}^{\mathrm{C}}_{\mathrm{T}}\boldsymbol{r}_1,{}^{\mathrm{C}}_{\mathrm{T}}\boldsymbol{r}_2,{}^{\mathrm{C}}_{\mathrm{T}}\boldsymbol{T}]{}^{\mathrm{t}}\boldsymbol{P}. \tag{8} $$

It is assumed that the width of virtual rectangle is $\mathrm{P}_1\mathrm{P}_2=D$ and the proportion of length and width is r. Then, the target coordinates of the four virtual vertices can be given by:

$$ \begin{cases} {}^{\mathrm{t}}\boldsymbol{P}_1=[0,0,1]^{\mathrm{T}} \\ {}^{\mathrm{t}}\boldsymbol{P}_2=[D,0,1]^{\mathrm{T}} \\ {}^{\mathrm{t}}\boldsymbol{P}_3=[0,-rD,1]^{\mathrm{T}} \\ {}^{\mathrm{t}}\boldsymbol{P}_4=[D,-rD,1]^{\mathrm{T}}. \end{cases} \tag{9} $$

Their image coordinates and camera coordinates respectively are:

$$ \begin{cases} \boldsymbol{p}_i=[u_i,v_i,1]^{\mathrm{T}} \\ {}^{\mathrm{c}}\boldsymbol{P}_i=[{}^{\mathrm{C}}X_i,{}^{\mathrm{C}}Y_i,{}^{\mathrm{C}}Z_i]^{\mathrm{T}}, \end{cases} \quad i=1,2,3,4. \tag{10} $$

Substituting (9) and (10) into (8), we can have:

$$ \lambda_i\boldsymbol{p}_i={}^{\mathrm{p}}_{\mathrm{T}}\boldsymbol{M}{}^{\mathrm{t}}\boldsymbol{P}_i \quad i=1,2,3,4. \tag{11} $$

In (11),

$$ \begin{cases} \lambda_i={}^{\mathrm{C}}Z_i \\ {}^{\mathrm{p}}_{\mathrm{T}}\boldsymbol{M}={}^{\mathrm{p}}_{\mathrm{C}}\boldsymbol{M}[{}^{\mathrm{C}}_{\mathrm{T}}\boldsymbol{r}_1,{}^{\mathrm{C}}_{\mathrm{T}}\boldsymbol{r}_2,{}^{\mathrm{C}}_{\mathrm{T}}\boldsymbol{T}]. \end{cases} $$

From (11), we can obtain the matrix equation:

$$ [\boldsymbol{p}_1,\boldsymbol{p}_2,\boldsymbol{p}_3]\,diag(\lambda_1,\lambda_2,\lambda_3)={}^{\mathrm{p}}_{\mathrm{T}}\boldsymbol{M}\left[{}^{\mathrm{t}}\boldsymbol{P}_1,{}^{\mathrm{t}}\boldsymbol{P}_2,{}^{\mathrm{t}}\boldsymbol{P}_3\right]. \tag{12} $$

Because the target coordinates of points P_1, P_2 and P_3 are not on a same line, the matrix $\left[{}^{\mathrm{t}}\boldsymbol{P}_1 \quad {}^{\mathrm{t}}\boldsymbol{P}_2 \quad {}^{\mathrm{t}}\boldsymbol{P}_3\right]$ is non-singular. From (11) and (12), we have:

$$ \lambda_4\boldsymbol{p}_4=[\boldsymbol{p}_1,\boldsymbol{p}_2,\boldsymbol{p}_3]diag(\lambda_1,\lambda_2,\lambda_3)[{}^{\mathrm{t}}\boldsymbol{P}_1,{}^{\mathrm{t}}\boldsymbol{P}_2,{}^{\mathrm{t}}\boldsymbol{P}_3]^{-1}({}^{\mathrm{t}}\boldsymbol{P}_4). \tag{13} $$

Using (9), the four points P_1, P_2, P_3 and P_4 have the following characteristic:

$$ [{}^{\mathrm{t}}\boldsymbol{P}_1,{}^{\mathrm{t}}\boldsymbol{P}_2,{}^{\mathrm{t}}\boldsymbol{P}_3]^{-1}({}^{\mathrm{t}}\boldsymbol{P}_4)=[-1,1,1]^{\mathrm{T}}. \tag{14} $$

Because the image coordinates of points P_1, P_2, and P_3 are also not on a same line. The matrix $\left[\boldsymbol{p}_1 \quad \boldsymbol{p}_2 \quad \boldsymbol{p}_3\right]$ is also non-singular. Substituting (14) into (13), we have:

$$ \frac{1}{\lambda_4}[-\lambda_1,\lambda_2,\lambda_3]^{\mathrm{T}}=[\boldsymbol{p}_1,\boldsymbol{p}_2,\boldsymbol{p}_3]^{-1}\boldsymbol{p}_4. \tag{15} $$

Equation (15) is the projection constraint on rectangle. However, the information is not enough to reconstruct a rectangle. The projection constraint on circular points will be introduced.

In infinite plane (the Homogeneous coordinate is zero), the absolute conic is [22]:

$$ \boldsymbol{Q}^{\mathrm{T}}\boldsymbol{C}\boldsymbol{Q}=0. \tag{16} $$

In (16), the absolute conic $\boldsymbol{C}$ is an unit matrix. $\boldsymbol{Q}$ are the points on absolute conic. It is assumed that the image coordinates of $\boldsymbol{Q}$ are $\boldsymbol{q}$, using (6), we have:

$$ \tau\boldsymbol{q}=({}^{\mathrm{p}}_{\mathrm{C}}\boldsymbol{M})({}^{\mathrm{C}}_{\mathrm{T}}\boldsymbol{R})\boldsymbol{Q}. \tag{17} $$

Substituting (17) into (16), the image of absolute conic is:

$$ \boldsymbol{q}^{\mathrm{T}}\boldsymbol{M}_{\mathrm{Abs}}\boldsymbol{q}=0. \tag{18} $$

In (18),

$$ \boldsymbol{M}_{\mathrm{Abs}}=({}^{\mathrm{p}}_{\mathrm{C}}\boldsymbol{M}^{-\mathrm{T}})({}^{\mathrm{p}}_{\mathrm{C}}\boldsymbol{M}^{-1}). $$

$\boldsymbol{M}_{\mathrm{Abs}}$ is only relation to the intrinsic parameters of camera.

Circular points are the intersections of circle and infinite straight line. Circular points are imaginary and conjugate points. Its coordinates are:

$$ \begin{cases} \boldsymbol{Q}_1=[1,j,0,0]^{\mathrm{T}} \\ \boldsymbol{Q}_2=[1,-j,0,0]^{\mathrm{T}}. \end{cases} \tag{19} $$

Substituting (19) into (16), we can conclude that the circular points are on the absolute conic. i.e., the image of circular points are also on the image of absolute conic. Because of the circular points $Z=0$, using (11), the image coordinates of the circular points are:

$$ \tau_i\boldsymbol{q}_i={}^{\mathrm{p}}_{\mathrm{T}}\boldsymbol{M}\boldsymbol{Q}_i, \quad i=1,2. \tag{20} $$

Substituting (20) into (18), we can obtain the equation of circular points:

$$\boldsymbol{Q}_i^{\mathrm{T}}({}_{\mathrm{T}}^{\mathrm{p}}\boldsymbol{M}^{\mathrm{T}})(\boldsymbol{M}_{\mathrm{Abs}})({}_{\mathrm{T}}^{\mathrm{p}}\boldsymbol{M})\boldsymbol{Q}_i = 0. \tag{21}$$

Equation (21) is complex numbers that is equal to zero. The real part and imaginary part are all equal to zero. we have:

$$[1,0,0]({}_{\mathrm{T}}^{\mathrm{p}}\boldsymbol{M}^{\mathrm{T}})(\boldsymbol{M}_{\mathrm{Abs}})({}_{\mathrm{T}}^{\mathrm{p}}\boldsymbol{M})[0,1,0]^{\mathrm{T}} = 0. \tag{22}$$

Equation (22) is the final projection constraint on circular points. In order to combine the projection constraints on rectangle and circular points, it can be rewritten to the following equation by (9):

$$\frac{1}{rD^2}({}^{\mathrm{t}}\boldsymbol{P}_4 - {}^{\mathrm{t}}\boldsymbol{P}_3)^{\mathrm{T}}({}_{\mathrm{T}}^{\mathrm{p}}\boldsymbol{M}^{\mathrm{T}})(\boldsymbol{M}_{\mathrm{Abs}})({}_{\mathrm{T}}^{\mathrm{p}}\boldsymbol{M})({}^{\mathrm{t}}\boldsymbol{P}_4 - {}^{\mathrm{t}}\boldsymbol{P}_2) = 0. \tag{23}$$

Using (12) and (14), we have:

$$[\boldsymbol{p}_1,\boldsymbol{p}_2,\boldsymbol{p}_3][-\lambda_1,\lambda_2,\lambda_3]^{\mathrm{T}} = ({}_{\mathrm{T}}^{\mathrm{p}}\boldsymbol{M}){}^{\mathrm{t}}\boldsymbol{P}_4, \tag{24}$$

$$[\boldsymbol{0},\boldsymbol{p}_2,\boldsymbol{0}][-\lambda_1,\lambda_2,\lambda_3]^{\mathrm{T}} = ({}_{\mathrm{T}}^{\mathrm{p}}\boldsymbol{M}){}^{\mathrm{t}}\boldsymbol{P}_2, \tag{25}$$

$$[\boldsymbol{0},\boldsymbol{0},\boldsymbol{p}_3][-\lambda_1,\lambda_2,\lambda_3]^{\mathrm{T}} = ({}_{\mathrm{T}}^{\mathrm{p}}\boldsymbol{M}){}^{\mathrm{t}}\boldsymbol{P}_3. \tag{26}$$

Then, subtracting (25) with (24) and subtracting (26) with (24), we have:

$$\begin{cases} {}_{\mathrm{T}}^{\mathrm{p}}\boldsymbol{M}({}^{\mathrm{t}}\boldsymbol{P}_4 - {}^{\mathrm{t}}\boldsymbol{P}_2) = [\boldsymbol{p}_1,\boldsymbol{0},\boldsymbol{p}_3][-\lambda_1,\lambda_2,\lambda_3]^{\mathrm{T}} \\ {}_{\mathrm{T}}^{\mathrm{p}}\boldsymbol{M}({}^{\mathrm{t}}\boldsymbol{P}_4 - {}^{\mathrm{t}}\boldsymbol{P}_3) = [\boldsymbol{p}_1,\boldsymbol{p}_2,\boldsymbol{0}][-\lambda_1,\lambda_2,\lambda_3]^{\mathrm{T}}. \end{cases} \tag{27}$$

Substituting (15) and (27) into (23), the equation of image coordinates is:

$$\begin{aligned} &\boldsymbol{p}_4^{\mathrm{T}}[\boldsymbol{p}_1,\boldsymbol{p}_2,\boldsymbol{p}_3]^{-\mathrm{T}}[\boldsymbol{p}_1,\boldsymbol{p}_2,\boldsymbol{0}]^{\mathrm{T}} \\ &\quad\times\boldsymbol{M}_{\mathrm{Abs}}[\boldsymbol{p}_1,\boldsymbol{0},\boldsymbol{p}_3][\boldsymbol{p}_1,\boldsymbol{p}_2,\boldsymbol{p}_3]^{-1}\boldsymbol{p}_4 \\ &= 0. \end{aligned} \tag{28}$$

Equation (28) fuses the two projection constraints on rectangle and circular points. It will be used for rectangle reconstruction.

From the image of partial rectangle, three image lines $\boldsymbol{l}_i(\rho_i,\theta_i), i = 1,2,3$ have been extracted by image processing. The image coordinate $\boldsymbol{p}_1$ of point P_1 is the intersection of lines l_1 and l_3. The image coordinate $\boldsymbol{p}_2$ of point P_2 is the intersection of lines l_1 and l_2. From (3), the image coordinates are:

$$\begin{cases} \boldsymbol{p}_1 = \left[\frac{\sin\theta_3\rho_1-\sin\theta_1\rho_3}{\cos\theta_1\sin\theta_3-\sin\theta_1\cos\theta_3}, \frac{\cos\theta_3\rho_1-\cos\theta_1\rho_3}{\sin\theta_1\cos\theta_3-\cos\theta_1\sin\theta_3}, 1\right]^{\mathrm{T}} \\ \boldsymbol{p}_2 = \left[\frac{\sin\theta_2\rho_1-\sin\theta_1\rho_2}{\cos\theta_1\sin\theta_2-\sin\theta_1\cos\theta_2}, \frac{\cos\theta_2\rho_1-\cos\theta_1\rho_2}{\sin\theta_1\cos\theta_2-\cos\theta_1\sin\theta_2}, 1\right]^{\mathrm{T}}. \end{cases} \tag{29}$$

Choosing an arbitrary image coordinate on line l_3 as the $\boldsymbol{p}_3$ of virtual point P_3, i.e.,

$$\boldsymbol{p}_3 = \left[\frac{\rho_3 - v_3\sin\theta_3}{\cos\theta_3}, v_3, 1\right]^{\mathrm{T}}. \tag{30}$$

Then, the image coordinate $\boldsymbol{p}_4$ of virtual point P_4 can be derived from (28) and the image line $\boldsymbol{l}_2(\rho_2,\theta_2)$:

$$\begin{cases} \boldsymbol{p}_4^{\mathrm{T}}\boldsymbol{N}\boldsymbol{p}_4 = 0 \\ [\cos\theta_2, \sin\theta_2, -\rho_2]\boldsymbol{p}_4 = 0. \end{cases} \tag{31}$$

In (31),

$$\boldsymbol{N} = [\boldsymbol{p}_1,\boldsymbol{p}_2,\boldsymbol{p}_3]^{-\mathrm{T}}[\boldsymbol{p}_1,\boldsymbol{p}_2,\boldsymbol{0}]^{\mathrm{T}}\boldsymbol{M}_{\mathrm{Abs}}[\boldsymbol{p}_1,\boldsymbol{0},\boldsymbol{p}_3][\boldsymbol{p}_1,\boldsymbol{p}_2,\boldsymbol{p}_3]^{-1}.$$

Then, a whole virtual rectangle in image coordinate system is reconstructed by (29), (30) and (31). If the virtual rectangle in target coordinate system can be reconstructed, the question of pose measurement will be solved. In the following section, the structured point light will be used to reconstruct the virtual rectangle in target coordinate system.

4.2.2 The reconstruction of virtual rectangle in target coordinate system

From (4), if the depth information $\lambda_i(i = 1,2,3,4)$ are known, the camera coordinate ${}^{\mathrm{c}}\boldsymbol{P}_i(i = 1,2,3,4)$ will be obtained. Because the image coordinates of the virtual rectangle have been reconstructed, by (15), we will have:

$$[-\lambda_1,\lambda_2,\lambda_3]^{\mathrm{T}} = \lambda_4[\boldsymbol{p}_1,\boldsymbol{p}_2,\boldsymbol{p}_3]^{-1}\boldsymbol{p}_4. \tag{32}$$

In (32), only the depth information λ_4 is unknown, the structured point light will be used to compute it. In camera coordinate system, the structured point light ${}^{\mathrm{c}}\boldsymbol{P}_5$ is in the plane determined by the virtual rectangle:

$$[m,n,p]\begin{bmatrix} {}^{\mathrm{C}}X_5 \\ {}^{\mathrm{C}}Y_5 \\ {}^{\mathrm{C}}Z_5 \end{bmatrix} = 1. \tag{33}$$

In (33), the normal vector of plane is:

$$[m,n,p] = [1,1,1]\left[{}^{\mathrm{c}}\boldsymbol{P}_1, {}^{\mathrm{c}}\boldsymbol{P}_2, {}^{\mathrm{c}}\boldsymbol{P}_3\right]^{-1}. \tag{34}$$

Using (4), we have:

$$\left[{}^{\mathrm{c}}\boldsymbol{P}_1, {}^{\mathrm{c}}\boldsymbol{P}_2, {}^{\mathrm{c}}\boldsymbol{P}_3\right] = {}_{\mathrm{C}}^{\mathrm{p}}\boldsymbol{M}^{-1}\left[-\boldsymbol{p}_1,\boldsymbol{p}_2,\boldsymbol{p}_3\right] diag(-\lambda_1,\lambda_2,\lambda_3). \tag{35}$$

Using (32), we have:

$$diag(-\lambda_1,\lambda_2,\lambda_3) = \lambda_4 diag(\left[\boldsymbol{p}_1,\boldsymbol{p}_2,\boldsymbol{p}_3\right]^{-1}\boldsymbol{p}_4). \tag{36}$$

Substituting (35) and (36) into (34), the normal vector of the plane can be expressed as:

$$\begin{aligned} [m,n,p] = &\frac{1}{\lambda_4}[1,1,1]diag^{-1}([\boldsymbol{p}_1,\boldsymbol{p}_2,\boldsymbol{p}_3]^{-1}\boldsymbol{p}_4) \\ &\times[-\boldsymbol{p}_1,\boldsymbol{p}_2,\boldsymbol{p}_3]^{-1}({}_{\mathrm{C}}^{\mathrm{p}}\boldsymbol{M}). \end{aligned} \tag{37}$$

From (33) and (37), if the camera coordinate ${}^{\mathrm{c}}\boldsymbol{P}_5$ of structured point light P_5 is known, the depth information λ_4 will be calculated.

The image coordinate $\boldsymbol{p}_5$ of structured point light P_5 has been extracted by image processing. Using (1) and (4), its camera coordinate is:

$$^{c}\boldsymbol{P}_5 = \lambda_5 {}^{p}_{C}\boldsymbol{M}^{-1}\boldsymbol{p}_5 = {}^{S}Z({}^{C}_{S}\boldsymbol{r}_3) + {}^{C}_{S}\boldsymbol{T}. \tag{38}$$

From (38), the λ_5 and ${}^{S}Z$ can be solved as:

$$\begin{bmatrix} \lambda_5 \\ {}^{S}Z \end{bmatrix} = (\boldsymbol{M}_5\boldsymbol{M}_5^{T})^{-1}\boldsymbol{M}_5^{T}({}^{C}_{S}\boldsymbol{T}). \tag{39}$$

In (39),

$$\boldsymbol{M}_5 = [{}^{p}_{C}\boldsymbol{M}^{-1}\boldsymbol{p}_5, -{}^{C}_{S}\boldsymbol{r}_3].$$

Substituting (39) into (38), the camera coordinate $^{c}\boldsymbol{P}_5$ is:

$$^{c}\boldsymbol{P}_5 = [1,0](\boldsymbol{M}_5\boldsymbol{M}_5^{T})^{-1}\boldsymbol{M}_5^{T}({}^{C}_{S}\boldsymbol{T}){}^{p}_{C}\boldsymbol{M}^{-1}\boldsymbol{p}_5. \tag{40}$$

Then, substituting (37) and (40) into (33), the parameter λ_4 can be computed by:

$$\begin{aligned}\lambda_4 =& [1,1,1]diag^{-1}([\boldsymbol{p}_1,\boldsymbol{p}_2,\boldsymbol{p}_3]^{-1}\boldsymbol{p}_4)[-\boldsymbol{p}_1,\boldsymbol{p}_2,\boldsymbol{p}_3]^{-1}({}^{p}_{C}\boldsymbol{M}) \\ & \times [1,0](\boldsymbol{M}_5\boldsymbol{M}_5^{T})^{-1}\boldsymbol{M}_5^{T}({}^{C}_{S}\boldsymbol{T}){}^{p}_{C}\boldsymbol{M}^{-1}\boldsymbol{p}_5.\end{aligned} \tag{41}$$

After that, substituting λ_4 back into (32) to get $\lambda_i (i = 1,2,3)$. Now, the camera coordinates are:

$$^{c}\boldsymbol{P}_i = \lambda_i({}^{p}_{C}\boldsymbol{M}^{-1})\boldsymbol{p}_i, \quad i = 1,2,3,4. \tag{42}$$

In Euler space, the distance between two points in different coordinate systems are equal to each other, i.e., the length and width of the virtual rectangle in target coordinate system can be computed by the camera coordinate system:

$$\begin{cases} rD = \frac{1}{2}(\|^{c}\boldsymbol{P}_1 - {}^{c}\boldsymbol{P}_3\| + \|^{c}\boldsymbol{P}_2 - {}^{c}\boldsymbol{P}_4\|) \\ D = \frac{1}{2}(\|^{c}\boldsymbol{P}_1 - {}^{c}\boldsymbol{P}_2\| + \|^{c}\boldsymbol{P}_3 - {}^{c}\boldsymbol{P}_4\|). \end{cases} \tag{43}$$

Finally, substituting (43) into (9), the virtual rectangle in target coordinate system is reconstructed. Using the virtual rectangle, the relative pose of the non-cooperative target will be calculated.

4.3. The pose determination algorithm

Because of ${}^{T}Z = 0$, equation (5) can be simplified as:

$$^{c}\boldsymbol{P} = [{}^{C}_{T}\boldsymbol{r}_1, {}^{C}_{T}\boldsymbol{r}_2, {}^{C}_{T}\boldsymbol{T}]^{t}\boldsymbol{P}. \tag{44}$$

Using the virtual rectangle, the matrix equation of relative pose is:

$$\boldsymbol{A} = [{}^{C}_{T}\boldsymbol{r}_1, {}^{C}_{T}\boldsymbol{r}_2, {}^{C}_{T}\boldsymbol{T}]\boldsymbol{B}. \tag{45}$$

In (45),

$$\boldsymbol{A} = [^{c}\boldsymbol{P}_1, {}^{c}\boldsymbol{P}_2, {}^{c}\boldsymbol{P}_3, {}^{c}\boldsymbol{P}_4], \quad \boldsymbol{B} = [^{t}\boldsymbol{P}_1, {}^{t}\boldsymbol{P}_2, {}^{t}\boldsymbol{P}_3, {}^{t}\boldsymbol{P}_4]$$

Because the matrices $\boldsymbol{A}$ and $\boldsymbol{B}$ are not full rank, based on the least square method, the solution of the relative pose equation (45) is:

$$[{}^{C}_{T}\boldsymbol{r}_1, {}^{C}_{T}\boldsymbol{r}_2, {}^{C}_{T}\boldsymbol{T}] = \boldsymbol{A}\boldsymbol{B}^{T}(\boldsymbol{B}\boldsymbol{B}^{T})^{-1}. \tag{46}$$

Because the rotation matrix ${}^{C}_{T}\boldsymbol{R}$ is an orthonormal unit matrix, the third column vector is:

$${}^{C}_{T}\boldsymbol{r}_3 = {}^{C}_{T}\boldsymbol{r}_1 \times {}^{C}_{T}\boldsymbol{r}_2. \tag{47}$$

Using (7), (46) and (47), the relative rotation angles between target and camera coordinate systems are:

$$\begin{bmatrix} \alpha \\ \beta \\ \gamma \end{bmatrix} = \begin{bmatrix} \arcsin(-{}^{C}_{T}R_{23}) \\ \arctan({}^{C}_{T}R_{13}/{}^{C}_{T}R_{33}) \\ \arctan({}^{C}_{T}R_{21}/{}^{C}_{T}R_{22}) \end{bmatrix}. \tag{48}$$

The relative position between target and camera coordinate systems is:

$$\boldsymbol{T} = {}^{C}_{T}\boldsymbol{T}. \tag{49}$$

Above all, the key process of pose determination for non-cooperative target satellite is to separately reconstruct a whole virtual rectangle in image, camera and target coordinate systems. Based on the virtual rectangle, the relative pose between space robot and non-cooperative target is computed by the least square method. In the following section, the proposed method will be verified by a semi-physical simulation system.

5. SIMULATION AND VERIFICATION

5.1. A semi-physical vision simulation system

To verify the proposed method, several representative simulations are presented in this section. All simulations are completed by a semi-physical vision simulation system. An industrial CCD camera is introduced to the simulation system to simulate the real process of image acquisition.

The configuration of the semi-physical vision simulation system is shown in Fig. 9. The advantage of the semi-physical simulation system is that the relative pose between structured light vision system and non-cooperative target is known exactly. By comparing the known pose with the computed pose, the proposed method can be verified effectively.

The simulation system is composed of four hardware parts, as shown in Fig. 10. It includes a relative dynamics and GNC computer, an image generating and display computer, an image processing and pose determination computer, and an industrial CCD camera. Their functions are:

A. Relative dynamics and GNC computer

The relative dynamics includes relative orbit dynamics and attitude dynamics. The relative orbit dynamics is C-W

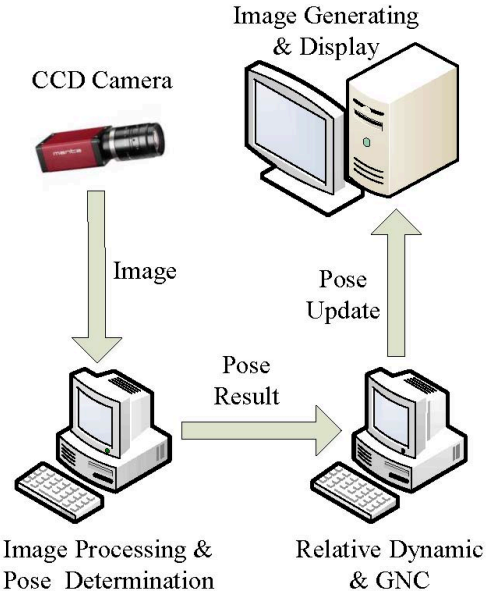

Fig. 9. The configuration of semi-physical vision simulation system.

Fig. 10. The hardware of semi-physical vision simulation system.

equations. i.e.,

$$\begin{cases} \ddot{x} = 2n\dot{z} + a_x \\ \ddot{y} = -n^2 y + a_y \\ \ddot{z} = -2n\dot{x} + 3n^2 z + a_z. \end{cases} \tag{50}$$

In (50), $[x, y, z]^{\mathrm{T}}$ is the relative motion between the space robotic system and the non-cooperative target satellite. $[a_x, a_y, a_z]^{\mathrm{T}}$ is the external acceleration added on the space robotic system. n is the orbital angular seed of the non-cooperative target satellite.

The attitude dynamic equations can be expressed in the well-known form:

$$\boldsymbol{I}\dot{\boldsymbol{\omega}} = -\boldsymbol{\omega} \times \boldsymbol{I}\boldsymbol{\omega} + \boldsymbol{\tau}. \tag{51}$$

In (51), $\boldsymbol{I}$ is the rotational inertia of spacecraft. $\boldsymbol{\omega}$ is the angular velocity of spacecraft. $\boldsymbol{\tau}$ is the torque, including control torque and disturbance torque.

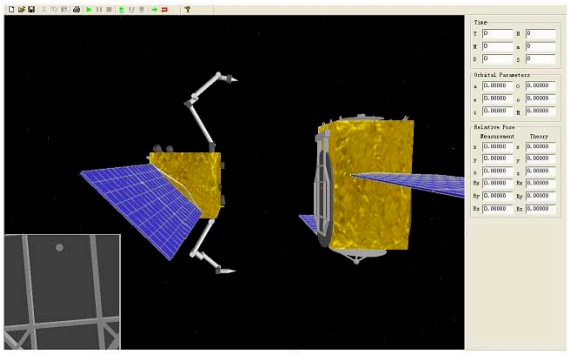

Fig. 11. The main scenario of relative motion between space robotic system and non-cooperative target satellite.

The main scenario of relative motion between the space robotic system and non-cooperative target satellite is described by OpenGL, as shown in Fig. 11.

The functions of GNC are the attitude and position tracking control based on the results of relative pose determination.

B. Image generating and display computer.

Using the data of relative motion between space robotic system and non-cooperative target satellite, the computer generates the image of non-cooperative target satellite by a virtual camera in OpenGL. The virtual camera is built by the parameters in Table 1. The virtual camera simulates a real vision camera mounted on the space robotic system. Meanwhile, the image of point light is also created by the virtual camera. The image that includes a partial rectangle of the non-cooperative target satellite and the point light has been shown in Fig. 5. Then, the image will be projected on a LCD that can be photographed by a CCD camera.

C. Industrial CCD camera

A real camera is applied in the simulation system as the physical component in control loop. It stands for a vision camera on the space robotic system. The process of pose determination can be realized truly. An industrial CCD camera from AVT (A Germany Company) is selected as the real camera. Its main specification is shown in Table 3.

Because the real camera does not coincide with the virtual camera in Euler space, the relationship between the two cameras should be calibrated. As the same as (4), the relationship between virtual camera coordinate system

Table 3. The main specification of the AVT camera.

	Parameter	Specification
(1)	Type	Manta G-146B/C
(2)	Resolution	1388×1038
(3)	Sensor type	CCD
(4)	Sensor size	1/2”
(5)	Output	Bits depth:8 12 Gray:Mono8/16 RGB:RGB24/BGR24
(6)	Interface	IEEE802.3-1000baseT

and virtual image coordinate system is:

$$\lambda_{\mathrm{Vir}} \begin{bmatrix} u_{\mathrm{Vir}} \\ v_{\mathrm{Vir}} \\ 1 \end{bmatrix} = {}^{\mathrm{p}}_{\mathrm{C}}\boldsymbol{M}_{\mathrm{Vir}} \begin{bmatrix} X_{\mathrm{Vir}} \\ Y_{\mathrm{Vir}} \\ Z_{\mathrm{Vir}} \end{bmatrix}. \tag{52}$$

In (52), ${}^{\mathrm{p}}_{\mathrm{C}}\boldsymbol{M}_{\mathrm{Vir}}$ that is known is the intrinsic parameter of virtual camera.

The relationship between the virtual image coordinate system and the real camera coordinate system is:

$$\begin{bmatrix} {}^{\mathrm{C}}X \\ {}^{\mathrm{C}}Y \\ {}^{\mathrm{C}}Z \end{bmatrix} = \boldsymbol{M}_{\mathrm{Ex}} \begin{bmatrix} d_{\mathrm{LCD}} & 0 & 0 \\ 0 & d_{\mathrm{LCD}} & 0 \\ 0 & 0 & 1 \end{bmatrix} \begin{bmatrix} u_{\mathrm{Vir}} \\ v_{\mathrm{Vir}} \\ 1 \end{bmatrix}. \tag{53}$$

In (53), d_{LCD} is the physical size of LCD pixel. $\boldsymbol{M}_{\mathrm{Ex}}$ is the external matrix between real camera and LCD. Substituting (52) and (53) into (4), the relationship between virtual camera coordinate system and real image coordinate system is:

$$\lambda\lambda_{\mathrm{Vir}} \begin{bmatrix} u \\ v \\ 1 \end{bmatrix} = {}^{\mathrm{p}}_{\mathrm{Vir}}\boldsymbol{M} \begin{bmatrix} X_{\mathrm{Vir}} \\ Y_{\mathrm{Vir}} \\ Z_{\mathrm{Vir}} \end{bmatrix}. \tag{54}$$

In (54),

$${}^{\mathrm{p}}_{\mathrm{Vir}}\boldsymbol{M} = {}^{\mathrm{p}}_{\mathrm{C}}\boldsymbol{M}\boldsymbol{M}_{\mathrm{Ex}} \begin{bmatrix} d_{\mathrm{LCD}} & 0 & 0 \\ 0 & d_{\mathrm{LCD}} & 0 \\ 0 & 0 & 1 \end{bmatrix} {}^{\mathrm{p}}_{\mathrm{C}}\boldsymbol{M}_{\mathrm{Vir}}.$$

${}^{\mathrm{p}}_{\mathrm{Vir}}\boldsymbol{M}$ is the transform matrix between virtual camera coordinate system and real image coordinate system. It is the theoretical principle of the semi-physical vision simulation system. It can be calibrated by circular features, as shown in Fig. 12. The calibration method is given in [23].

D. Image processing and pose determination computer

The computer receives the gray images of non-cooperative target satellite from the CCD camera and does image processing by the method in section 3.2. The software of OpenCV (Open Computer Vision) are applied to process the gray images. Then, the pose determination will be executed by the proposed method in section 4. The results will be sent to the relative dynamic and GNC computer to form the closed loop control system.

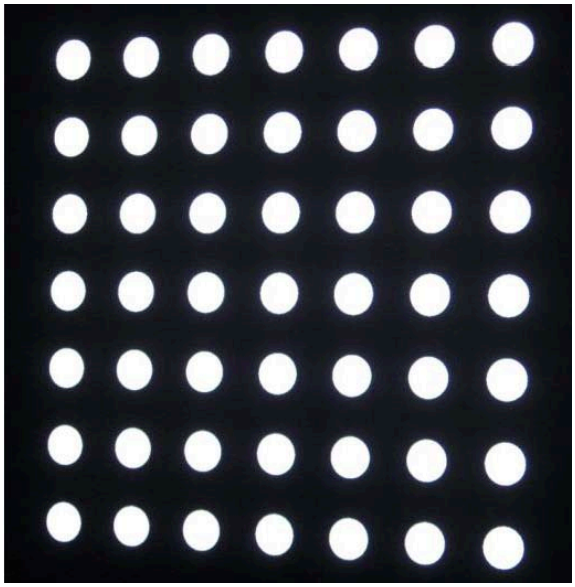

Fig. 12. The circular features for calibration.

5.2. Verification

5.2.1 Scenario 1: Pose measurement through a planned path

It is assumed that the space robotic system has performed a proximity to the non-cooperative target satellite at the relative range of 2 meters. The current situation is that the rectangle used for pose measurement is beyond the FOV of camera and the navigation method is invalid. In the following approach to the berthing position at 1 meter, the pose determination method proposed in this paper will be applied to navigate sequentially. The initial relative attitude and position between space robotic system and non-cooperative target satellite are given:

$$\begin{cases} [\alpha, \beta, \gamma] = [-7.4^\circ, -6.6^\circ, 6.3^\circ] \\ {}^{\mathrm{C}}_{\mathrm{T}}\boldsymbol{T} = [-425.1\ \mathrm{mm},\ 363.5\ \mathrm{mm},\ 1642.6\ \mathrm{mm}]^{\mathrm{T}}. \end{cases} \tag{55}$$

To perform on-orbit operations, the space robotic system will close to the non-cooperative target satellite at berthing position. The desired relative pose is:

$$\begin{cases} [\alpha, \beta, \gamma] = [0^\circ, 0^\circ, 0^\circ] \\ {}^{\mathrm{C}}_{\mathrm{T}}\boldsymbol{T} = [-383.9\ \mathrm{mm},\ 480.1\ \mathrm{mm},\ 999.6\ \mathrm{mm}]^{\mathrm{T}}. \end{cases} \tag{56}$$

The calibration result of matrix ${}^{\mathrm{p}}_{\mathrm{Vir}}\boldsymbol{M}$ is:

$${}^{\mathrm{p}}_{\mathrm{Vir}}\boldsymbol{M} = \begin{bmatrix} 1.000 & -4.556 \times 10^{-3} & 0.518 \\ 3.853 \times 10^{-4} & 0.999 & 0.513 \\ -6.417 \times 10^{-6} & -9.821 \times 10^{-6} & 2.002 \times 10^{-3} \end{bmatrix}. \tag{57}$$

Through 200 control periods, the space robotic system will be at the berthing position. In every control period, the monocular structured light vision system will provide relative pose information to the GNC. The relative attitude

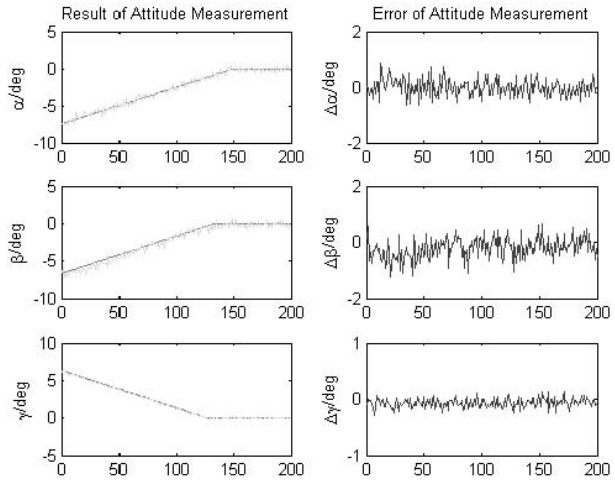

Fig. 13. The results of relative attitude and errors.

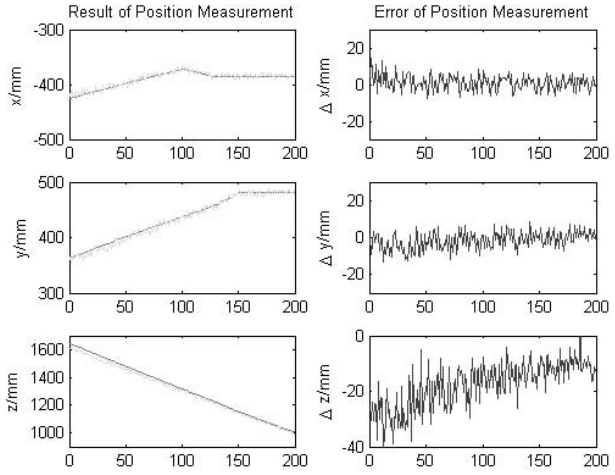

Fig. 14. The results of relative position and errors.

and position tracking trajectory and the tracking errors are shown in Figs. 13 and 14, respectively. From the simulation results, the proposed method for pose determination of non-cooperative target satellite is effective and feasible. Compared the three angles, the angle γ is more precise than the other two angles. For a rectangle, the pixel variation caused by angle γ is more than that caused by the other two angles in the same rotation. i.e., angle γ is more sensitive to pixel variation. Compared the three positions, the position error of the axis Z is a little larger than that of the other two axes. The reason is that the relative motion along the normal direction of a rectangle plane (the direction along the LOS) is relatively difficult to be detected. The depth information is lost by the projection from 3D to 2D.

5.2.2 Scenario 2: Pose measurement under different mounted matrix between camera and point light

Analyzing the pose measurement algorithm, the error sources of the proposed method are: (a) The precision of intrinsic parameters ${}^{\mathrm{p}}_{\mathrm{C}}\boldsymbol{M}$ and mounted matrix ${}^{\mathrm{C}}_{\mathrm{S}}\boldsymbol{M}$ which can be calibrated. (b) The precision of inputs $l_i(\rho_i,\theta_i)$ and $\boldsymbol{p}_5$ which can be extracted by image processing. The error sources can be simulated by the semi-physical vision simulation system except the mounted matrix ${}^{\mathrm{C}}_{\mathrm{S}}\boldsymbol{M}$. It does not exist in the simulation system. Therefore, the errors of matrix ${}^{\mathrm{C}}_{\mathrm{S}}\boldsymbol{M}$ are added separately.

Table 4. The random errors of mounted matrix.

	Error	Case A1	Case A2
(1)	$\Delta\alpha_{\mathrm{S}},\Delta\beta_{\mathrm{S}},\Delta\gamma_{\mathrm{S}}(^\circ)$	0.1,0.1,0.1	0.2,0.2,0.2
(2)	$\Delta X_{\mathrm{S}},\Delta Y_{\mathrm{S}},\Delta Z_{\mathrm{S}}(mm)$	5,5,5	10,10,10

Table 5. The maximum errors under different calibrations.

	Error	Case A1	Case A2
(1)	$\Delta\alpha(^\circ)$	0.517	0.558
(2)	$\Delta\beta(^\circ)$	0.634	0.603
(3)	$\Delta\gamma(^\circ)$	0.167	0.154
(4)	$\Delta T_{\mathrm{X}}(mm)$	7.85	7.17
(5)	$\Delta T_{\mathrm{Y}}(mm)$	6.93	8.80
(6)	$\Delta T_{\mathrm{Z}}(mm)$	35.9	38.3

Table 6. The three different mounted positions.

	Position	Case B1	Case B2	Case B3
(1)	${}^{\mathrm{C}}_{\mathrm{S}}\boldsymbol{T}(mm)$	$[0,-300,0]^{\mathrm{T}}$	$[0,-500,0]^{\mathrm{T}}$	$[0,-700,0]^{\mathrm{T}}$

A. Simulations in different calibration errors of the mounted matrix

In theoretical design, the matrix ${}^{\mathrm{C}}_{\mathrm{S}}\boldsymbol{M}$ is given by (1). The rotation matrix ${}^{\mathrm{C}}_{\mathrm{S}}\boldsymbol{R}$ is an unit matrix. The rotation errors are $\Delta\alpha_{\mathrm{S}}$, $\Delta\beta_{\mathrm{S}}$ and $\Delta\gamma_{\mathrm{S}}$. The translation vector ${}^{\mathrm{C}}_{\mathrm{S}}\boldsymbol{T}$ with calibration errors is:

${}^{\mathrm{C}}_{\mathrm{S}}\boldsymbol{T}=[\Delta X_{\mathrm{S}},-500mm+\Delta Y_{\mathrm{S}},\Delta Z_{\mathrm{S}}]^{\mathrm{T}}$

Two different random errors of matrix ${}^{\mathrm{C}}_{\mathrm{S}}\boldsymbol{M}$ are given in Table 4. The two different states will be experimented at initial relative pose. The proposed algorithm will be executed about 1,000 times in each state. The maximum errors of these experiments are shown in Table 5. From the results, it is concluded that the mounted matrix ${}^{\mathrm{C}}_{\mathrm{S}}\boldsymbol{M}$ has more effect on the position than that on the attitude.

B. Simulations in different mounted position

Under the error situation of Case A1, three different mounted position are given to perform pose determination at initial relative pose, as shown in Table 6. The proposed algorithm will be also executed about 1,000 times in each state. The maximum errors of these experiments are shown in Table 7. From the results, the mounted position is bigger, the results of the pose determination are more precise. Especially, the improvement of position in axis Z is obvious.

The results of the several experiments by the semi-physical vision system show that the pose determination

Table 7. The maximum errors under different mounted positions.

	Error	Case B1	Case B2	Case B3
(1)	$\Delta\alpha(^\circ)$	0.540	0.517	0.484
(2)	$\Delta\beta(^\circ)$	0.624	0.634	0.588
(3)	$\Delta\gamma(^\circ)$	0.186	0.167	0.151
(4)	$\Delta T_X(mm)$	7.98	7.85	7.81
(5)	$\Delta T_Y(mm)$	7.12	6.93	6.95
(6)	$\Delta T_Z(mm)$	39.7	35.9	31.8

of non-cooperative target satellite based on the monocular structured light vision sensor is feasible and effective.

6. CONCLUSIONS

The GEO orbit is very important and useful but limited for human beings. Most GEO satellites are communication, navigation and weather satellites that are complicated and high-value. The failures of these GEO satellites will result in huge economic loss and other bad influences. Therefore, the OOS of GEO are playing more and more important role. Before the OOS of GEO becomes engineering, there will be some key technologies to be solved, such as non-cooperative target rendezvous and berthing, pose measurement, dexterous space manipulator, and target releasing, etc. In these key technologies, the pose measurement of non-cooperative target satellite is the precondition of berthing, capture and operation.

In this paper, a space robotic system for the OOS of GEO is introduced, and a relative pose measurement system is developed for berthing between the space robotic system and the non-cooperative target. The main contributions of the work can be summarized as follows:

(a) The design of monocular structured light vision sensor: The space robotic system that has two 7-DOF redundant manipulators, relative navigation and measurement subsystem and base subsystems is introduced firstly. It can serve most existing satellites in GEO. Based on the space robotic system, the monocular structured light vision sensor is designed. The designed system is composed of a single vision camera and a point light. The parameters of the camera and the point light are given in detail. Using the designed vision system, the space robotic system can measure the relative pose of non-cooperative target satellites by natural features.

(b) The algorithm of pose determination based on a partial rectangle: A partial rectangle on the non-cooperative target satellite whose size is unknown is chosen as the measurement object. The image of the partial rectangle with point light is obtained by the vision camera. And the image processing methods are presented in detail. It includes the image filter, point extraction and line extraction. Using these image information, a pose determination algorithm is proposed. The method combines the projection constraints on rectangle and circular points. Two whole virtual rectangles in image coordinate system and target coordinate system are reconstructed. Using the two whole virtual rectangles, the relative pose between space robotic system and non-cooperative target satellite is computed by least square method.

(c) The design of semi-physical vision simulation system: Because a physical camera is introduced to the simulation system, the reliability of the simulation system is improved. The simulation system is composed of the relative dynamic and GNC computer, the image processing and pose determination computer, the image generating and display computer and a industrial CCD camera. The simulation system is a hardware-in-loop system. It is more real than a full-digital simulation system. The semi-physical simulation results show that the relative pose determination method is effective. The method can be used to measure the non-cooperative target satellites with rectangular features. In the future, a semi-physical system with a real point light and a physical target model will be further developed to verify the pose determination method.

REFERENCES

[1] M. Tafazoli, "A study of on-orbit spacecraft failures," *Acta Astronautica*, vol. 64, no. 2, pp. 195-205, 2009. [click]

[2] A. Ellery, J. Kreisel, and B. Sommer, "The case for robotic on-orbit servicing of spacecraft: spacecraft reliability is a myth," *Acta Astronautica*, vol. 63, no. 5, pp. 632-648, 2008. [click]

[3] F. Sellmaier, J. Spurmann, and T. Boge, "On-orbit servicing missions at DLR / GSOC," *61st International Astronautical Congress*, Prague, CZ, 2010.

[4] G. Visentin and D. L. Brown, "Robotics for geostationary satellite servicing," *Robotics and Autonomous System*, vol. 23, no. 1-2, pp. 45-51, 1998. [click]

[5] L. Tarabini, J. Gil, F. Gandia, M. A. Molina, J. M. D. Cura, and G. Ortega, "Ground guided CX-OLEV rendezvous with uncooperative geostationary satellite,"*Acta Astronautica*, vol. 61, no. 1-6, pp. 312-325, 2007. [click]

[6] J. Obermark, G. Creamer, B. E. Kelm, W. Wagner, and C. G. Henshaw, "SUMO/FREND: vision system for autonomous satellite grapple,"*Proceedings of the SPIE - Sensors and Systems for Space Applications*, vol. 6555, 2007.

[7] K. Yoshida, "Engineering test satellite VII flight experiments for space robot dynamics and control,"*International Journal of Robotics Research*, vol. 22, no. 5, pp. 321-335, 2003. [click]

[8] T. Weismuller and M. Leinz, "GNC technology demonstrated by the orbital express autonomous rendezvous and capture sensor system,"*The Boeing Company, Anaheim, CA 92803*.

[9] T. A. Mulder, "Orbital express autonomous rendezvous and capture flight operations,"*Proc. of AIAA/AAS Astro Dynamics Specialist Conference and Exhibit*, Honolulu, Hawaii, 2008.

[10] M. Lichter and S. Dubowsky, "State, shape, and parameter estimation of space objects from range images,"*IEEE International Conference on Robotics and Automation (ICRA 2004)*, New Orleans, LA, 2004.

[11] P. Jasiobedski, M. Greenspan, and G. Roth, "Pose determination and tracking for autonomous satellite capture,"*Proceeding of the 6th International Symposium on Artificial Intelligence, Robotics and Automation in Space*, St-Hubert, Quebec, Canada, 2001.

[12] F. Terui, H. Kamimura, and S. Nishida, "Motion estimation to a failed satellite on orbit using stereo vision and 3D model matching,"*The 9th International Conference on Control, Automation, Robotics and Vision*, Singapore, 2006.

[13] X. D. Du, B. Liang, W. F. Xu, and Y. Qiu, "Pose measurement of large non-cooperative satellite based on collaborative cameras," *Acta Astronautica*, vol. 68, no. 11-12, pp. 2047-2065, 2011. [click]

[14] X. D. Du, B. Liang, W. F. Xu, and Y. Qiu, "A Universal On-orbit Servicing System Used in the Geostationary Orbit," *Advances in Space Research*, vol. 48, no. 1, pp. 95-119, 2011. [click]

[15] R. Choc and R. Jehn, "Classification of geosynchronous objects, issue 11," *European Space Agency, European Space Operations Centre, Space Debris Office*, 2009.

[16] D. X. Bi, F. T. Liu, and Q. Xue "New structured light vision sensor field calibration approach based on laser intersection lines," *Chinese Journal of Scientific Instrument*, vol. 30, no. 8, pp. 1697-1701, 2009.

[17] Y.-D. Shin, J.-H. Park, J.-H. Bae, and M.-H. Baeg, "A study on reliability enhancement for laser and camera calibration," *International Journal of Control, Automation, and Systems*, vol. 10, no. 1, pp. 109-116, 2012. [click]

[18] Z. Song, Y. Q. Chen, K. L. Moore, and L. Ma, "Application of the sparse hough transform for laser data line fitting and segmentation," *International Journal of Robotics and Automation*, vol. 21, no. 3, pp. 157-164, 2006.

[19] F. C. Wu, Z. Y. Hu, and H. J. Zhu, "Camera calibration with moving one-dimensional objects," *Pattern Recognition*, vol. 38, no. 5, pp. 755-765, 2005.

[20] X. Q. Meng and Z. Y. Hu, "A new easy camera calibration based on circular points," *Pattern Recognition*, vol. 36, no. 5, pp. 1155-1164, 2003.

[21] H. Gao, J. Liu, Y. Yu, and Y. Li, "Distance measurement of zooming image for a mobile robot," *International Journal of Control, Automation, and Systems*, vol. 11, no. 4, pp. 782-789, 2013. [click]

[22] N. Wang, D. Dong, and Y. Z. Fan, "A method of camera self calibration based on rectangles," *Journal of University of Science and Technology of China*, vol. 35, no. 5, pp. 693-700, 2005.

[23] X. D. Du, B. Liang, W. F. Xu, X. Q. Wang, and X. H. Gao, "A semi-physical simulation system for binocular vision guided rendezvous," *Proc. of The 12th International Conference on Control, Automation, Robotics and Vision*, Guangzhou, China, 2012.

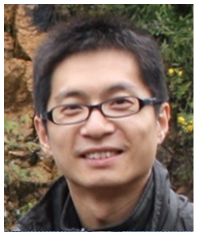

Xue-Hai Gao received his Ph.D. in Control Science and Engineering from Harbin Institute of Technology in 2015. His research interests include vision measurement, guidance, navigation and control of spacecraft.

Bin Liang received his Ph.D. in Instrument Science and Engineering from Tsinghua University in 1994. His research interests include space robot, control theory and applications.

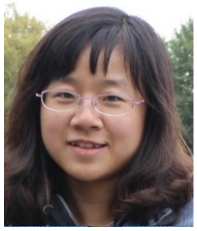

Le Pan received her M.S. in Detection Technology and Automatic Equipment from Hefei University of Technology in 2008. Her research interests include image processing, computer simulation.